GΩ Resistor for AC-coupled Amplifier in Audio Application

Junjie Wang

TU Delft

Faculty of Electrical Engineering, Mathematics and Computer Science

Delft University of Technology

GΩ Resistor for AC-coupled Amplifier in Audio Application

by

Junjie Wang

February 30, 2023

to obtain the degree of Master of Science in Microelectronics

at the Delft University of Technology

Student number: 5359023
Supervisors:
Asst. Prof. Dr. ir. Qinwen Fan
prof.dr.ir. F.P. Widdershoven

TU Delft Delft University of Technology

Abstract

AC-coupled amplifiers (ACCA) offer lower noise than traditional resistor feedback amplifiers, which benefits signal-to-noise ratio (SNR) for audio applications. Due to the DC isolation of the capacitor, a feedback resistor is needed to set the virtual ground of ACCA's amplifier. However, an external feedback resistor raises system noise and transforms the ACCA into a high-pass filter, impacting the audio bandwidth signal (20-20kHz). A GΩ resistor can shift the cut-off frequency outside the audio bandwidth while reducing noise. Various high-resistance resistor structures have been applied in biomedical readout integrated circuits (ICs), such as sequence detection, ECG, and EEG signal readout. However, the achieved signal-to-noise ratio and total harmonic distortion (THD) are unsuitable for audio applications. This thesis discusses different methods of making high-resistance resistors, such as duty-cycled resistors, switched-capacitor resistors, and pseudo resistors, exploring their possibility in audio applications. This work proposes an active current reducer structure with an equivalent resistance of 200GΩ (± 20%) and an output RMS noise of 2.1μV for ACCA. This circuit is built in the 180-nm BCD process achieving -106 dB to -116 dB THD and 96.7 dB SNR.

Index Terms – audio amplifier, high-resistance resistors, duty-cycled resistor, switched-capacitor resistor, pseudo resistor, active current reducers, total harmonic distortion (THD).

Acknowledgments

Osmanthus wine tastes the same as I remember... But where are those who share the memory?

My time at TU Delft has been wonderful but short. I arrived in Delft in the autumn of 2020 and will be leaving in the spring of 2023. Time has flown by so fast. As I look back on these past two and a half years, I have mixed feelings.

Firstly, I want to express my gratitude to my supervisor, Dr. ir. Qinwen Fan, for her invaluable help and guidance. Her patience and understanding have played a significant role in my thesis project, and I deeply appreciate her intuition and insight into analog design. She always provided valuable suggestions and pointed out key points in my design. Her advice on both my studies and personal life will be a treasure in my life. May your students everywhere.

Then, I will never forget the support from my family. I am grateful for their love, support, and encouragement throughout my life. They come from the countryside and may not fully understand what I do, but they always try their best and unconditionally support me whenever and whatever I need. I hope they always stay safe and healthy, and I miss them dearly.

Next, I would like to thank my part-time daily supervisor, Amirhossein Jouyaeian, as well as Rui Guan, Huajun Zhang, Heng Ma, Yihan Ouyang, and Zhongpeng Liang for their guidance and support throughout my master's thesis project. They were always willing to share their knowledge and experiences with me, not only in circuit design but also in life.

I also want to express my appreciation to Zuyao Chang for his help with my circuit design and Arthur Admiraal for his assistance with my presentation skills.

Lastly, I want to thank my friends here, especially Lai Wei, Zelin, Heqi, and many others for spending this wonderful two-and-a-half year with me. I also appreciate the companionship and help from Hankai, Chunsheng, Qiyi, Zhuohui, and Nick. During my time in the Netherlands, I made many friends and experienced new things with them. Communicating with them has broadened my horizons and knowledge. I would also like to thank my friends in China for their support and encouragement. I will never forget and will always cherish the experiences I had with them.

The memory of adventure in TU Delft will be the taste left in my osmanthus wine.

Junjie Wang
Delft
February 2023

Contents

Chapter 1 Introduction

1.1 Background and motivation

Traditional audio amplifiers set the closed-loop gain using a resistor feedback network (Figure 1.1(a)) [1]. However, the dynamic range of these audio amplifiers is limited due to thermal noise from the input resistor [2]. Decreasing the input resistor would lower the input impedance of the audio amplifier, which is undesirable in audio applications as it increases signal loss from the previous stage. The AC-coupled audio amplifier (ACCA) structure shown in Figure 1.1(b) has the potential to enhance the dynamic range of audio amplifiers. Capacitors naturally block DC signals without adding noise and power consumption, enabling ACCA to achieve low noise without reducing input impedance.

Nevertheless, the isolation of the DC signal by capacitor coupling prevents the operational amplifier's virtual ground voltage from being set [3]. The feedback capacitor also causes output saturation due to the charge stored on the capacitor. To set the virtual ground of the opamp and avoid output saturation, a feedback resistor (250 MΩ) is applied to form a first-order high-pass filter (HPF) in the previous structure [4] (Figure 1.1(c)). However, the relatively small feedback resistor pushes the HPF's cutoff frequency within the audio bandwidth. Chopping modulation preserves the audio signal by up-modulation, preventing it from being filtered by the HPF. The chopping frequency needs to be carefully selected to avoid intermodulation of the signals within the bandwidth. Up-modulation of the amplifier offset causes a ripple in the output, which is generally unacceptable. Ripple-reduction technique is applied to suppress ripple effectively, and an LC low-pass filter is the most straightforward way [3].

As depicted in Figure 1.1(d), a more straightforward structure could be achieved by applying a high-resistance feedback resistor that shifts the HPF's cut-off frequency outside the audio bandwidth. However, using traditional poly resistors to achieve GΩ or TΩ resistance is very area-consuming, which is often undesirable in integrated circuit design. This thesis aims to explore a method for designing high-resistance resistors and apply it in the audio field, serving as the starting point.

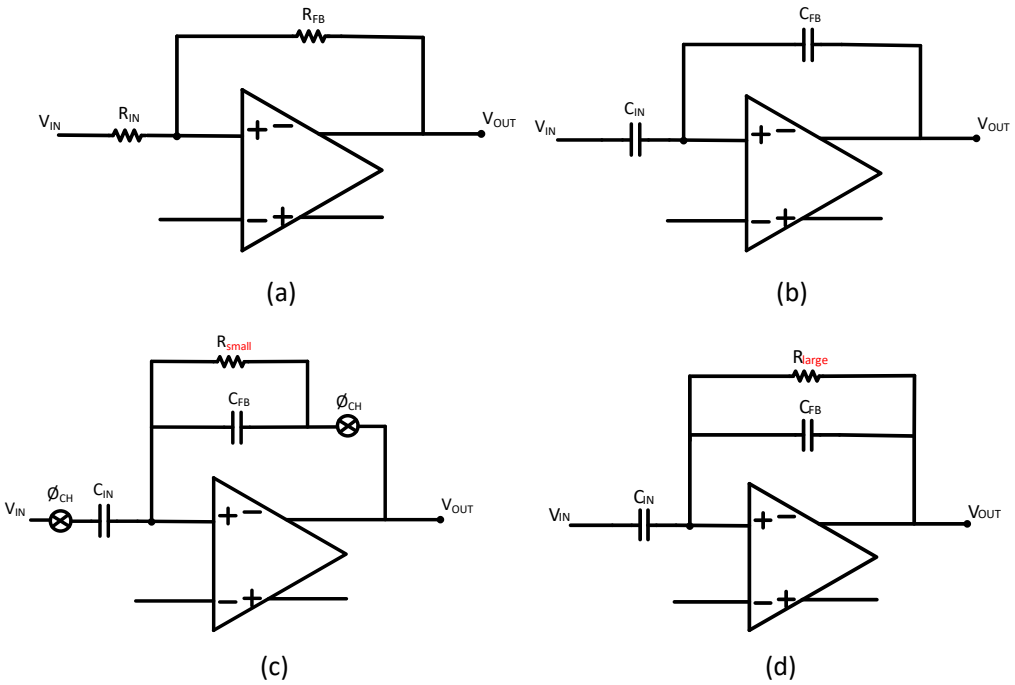

Figure 1.1 (a) resistor feedback audio amplifier; (b) AC-coupled amplifier[3]; (c) previous structure[4]; (d) High-resistance resistor feedback AC-coupled amplifier.

1.2 Spec for high-resistance resistor

This work focuses on exploring making a high-resistance resistor to simplify the previous ACCA structure, and the system spec (Table 1.1) references the previous work [4]. The closed-loop gain is determined by the input and output voltage supply, resulting in an 18dB gain. The input capacitance of the ACCA is set to 2.56 pF as a reference value, striking a balance between the capacitor's area consumption and the amplifier's input reference noise [4].

Table 1.1 Inherited system spec

Close loop gain (dB)	18
bandwidth	20-20kHz
Output RMS noise (μVrms)	8
SNR@100mV input (dB)	97
THD@-1dBFS (dB)	-113

The high-resistance resistor needs to meet specific requirements for the audio application. First, the resistance, which decides the cut-off frequency of the HPF by the equation $f_c = \frac{1}{2\pi R_{large} C_{fb}}$, affects the frequency response for ACCA. As shown in Figure

1.2, the red line presents the frequency response made by a higher-resistance feedback resistor compared to the others, achieving a flatter gain and phase frequency response in the audio bandwidth from 20 Hz to 20k Hz.

In audio applications, the signals within the audio bandwidth should be affected as little as possible by the HPF. As the cut-off frequency increases, the gain and phase shifts within the bandwidth increase (Figure 1.3). The tolerance for the cut-off frequency required to achieve a flat bandwidth frequency response is based on currently available audio systems on the market (Table 1.2).

Table 1.2 Gain shift and phase shift for advanced audio devices

	Gian shift (dB)	Phase shift (degree)
Iloud Precision 6 [5]	1	20
Genelec 8050B [6]	2	N/A
ICEpower 700AS2 [7]	3	35

The Iloud Precision 6 speaker, as a representative of consumer audio speakers, is capable of a 20-degree phase shift and a 1 dB gain shift within its bandwidth [5]. Other advanced audio devices, such as the Genelec 8050B [6], which has a gain shift of 2 dB, and the audio amplifier ICEpower 700AS2 achieve a 3 dB gain shift and a 35-degree phase shift [7].

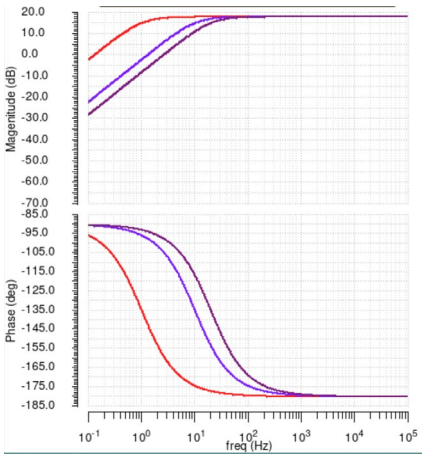

Figure 1.2 Frequency response for ACCA

In this project, the Iloud Precision 6 speaker serves as a reference for a high-quality audio system. The cut-off frequency of ACCA should be below 7.3Hz, implying that a 70 GΩ feedback resistor would be sufficient for the audio application in this project. We chose 2.5 Hz as the target for this academic research project, so a 200GΩ feedback resistor is needed.

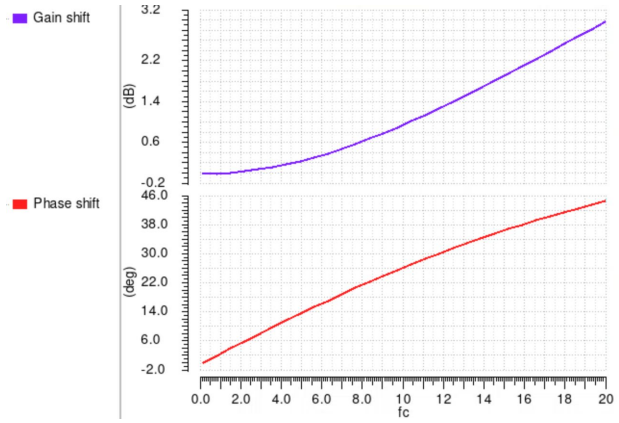

Figure 1.3 Gian shift and phase shift versus input frequency

In addition, noise is an essential consideration in audio applications. The previous structure has an output RMS noise of 8μV within audio bandwidth. Introducing a feedback resistor increases the total noise of the previous structure. The output RMS noise contribution from the feedback resistor is adjusted at 2 μV in order to reduce the impact of the noise contribution from the feedback resistor. The noise model of ACCA can be simplified as a first-order RC lowpass filter (Figure 1.4). The output RMS noise can be calculated by the equation (1.1)

$$\overline{V_{RMS,out}} = \sqrt{\int_{20}^{20k} \frac{4kTR_{fb}}{\left|1 + j2\pi fC_{fb}R_{fb}\right|^2} df} \tag{1.1}$$

Note that a 200 GΩ resistor typically generates 32 μV RMS noise at the output. The resistance should increase to 51 TΩ, or the feedback capacitor should be raised to 5 pF to attain 2 μV output RMS noise contribution. Both adjustments would result in a significant increase in chip area consumption. Thus, designing a 200 GΩ resistor with 2μV output RMS noise poses a challenge in this project.

Linearity is another crucial aspect of audio systems, often represented by total harmonic distortion (THD). The previous structure has a THD of -113 dB at -1dBFS, so linearity is expected to be maintained when applying this high-resistance resistor to the ACCA. Consequently, the THD of the ACCA should be less than -113dB at -1dBFS.

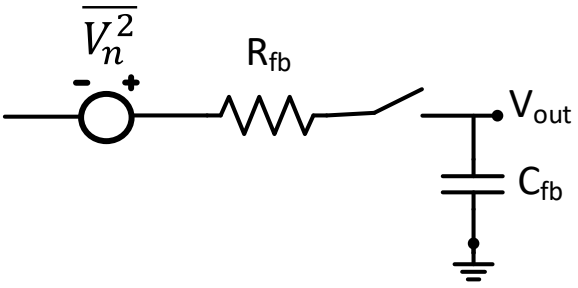

Figure 1.4 simplified noise model of the high-resistance resistor in ACC

1.3 State of the art for high-resistance resistor

Many solutions have been proposed to achieve high-resistance resistors, such as pseudo resistors [8-12], duty-cycled resistors (DSR) [13-17], and switched-capacitor resistors (SCR) [18-22]. These high-resistance resistors are widely used in biomedical readout integrated circuits(ICs) which require low power consumption, small area, and multiple channels [23]. In sequence detection, DNA sequences passing through a nanopore generate biological current information of approximately 100 pA [24]. A high-resistance resistor feedback transimpedance amplifier could convert this small input current signal into voltage signals for further processing. Using traditional poly resistors significantly limits the number of channels. Pseudo resistors (Figure 1.4(a)), which achieve high resistance by one or several diode-connected PMOS, can increase the number of channels on a chip by dozens of times. A 50 MΩ pseudo resistor used as a feedback resistor in a transimpedance amplifier for reading DNA sequences achieved a 30.6 dB SNR [9]. ECG signals require low-noise, low-power biosignal amplifiers to read out signals from the millihertz to the kilohertz range while suppressing large DC offsets generated by the electrode-tissue interface. An ACCA with a 0.1 TΩ pseudo resistor as feedback achieved a cutoff frequency of 0.025 Hz, -40 dB THD, and 60.6 SNR [8]. Pseudo resistors are nonlinear and highly sensitive to process and temperature variations [12], making them challenging to use in audio applications. Several structures have been proposed to enhance the performance of pseudo resistors, such as back-to-back structures [11] or active structures [25]. Active current-reducer (ACR), a type of active pseudo resistor structure (Figure 1.5(b)), has been proposed to further improve performance. Chapter 2 will discuss the applicability of these structures to this project.

Duty-cycled resistors (Figure 1.5(c)), which control the average current flowing through the resistor by adjusting the switch duty cycle, offer PVT robustness and linearity compared to pseudo-resistors. A 420 MΩ and 20 GΩ duty-cycled resistor were used to create an RC low-pass filter and integrator for processing ECG signals, resulting in a 66 dB SNR and -74 dB THD [14][16]. The maximum achievable resistance of a duty-cycled resistor is limited by the sampling frequency and parasitic capacitance [14]. The following chapters will discuss the feasibility of using a duty-cycled resistor in this project.

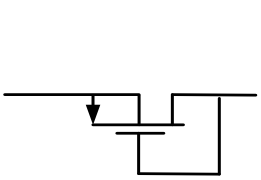

(a)

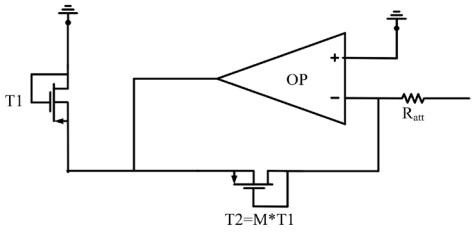

(b)

(c) (d)

Figure 1.5 (a) Pseudo resistor; (b) Active current-reducer[25]; (c) Duty-cycled resistor; (d) Switched-capacitor resistor

Switched capacitor resistors (Figure 1.5(d)) are formed by adjusting the charging and discharging ratio on the capacitor by switches. In 2021, a 100 TΩ switched capacitor resistor was applied as a feedback resistor in an acoustic amplifier, achieving an SNR of 67.5 dB [21]. We will discuss whether switched capacitor resistors can be applied in this project in Chapter 2.

Many methods for implementing high-resistance resistors are applied in biomedical readout integrated circuits, but the achieved THD and SNR are relatively low for audio applications. The specifications of this project and the current status of the art are shown in Table 1.3.

Table 1.3 Target Specifications

	This Work	03-JSSC[8]	12-Sensors and Actuators[9]	17-JSSC[14]	20-Centurelli [16]	21-VLSI [21]
Resistor Structure	TBD[I]	pseudo resistor	pseudo resistor	Duty-cycled resistor	Duty-cycled resistor	SCR[II]
Architecture[III]	ACCA	ACCA	Rf-TIA	Integrator	RC-filter	ACCA
Application[IV]	Audio application	ECG	DNA	ECG	ECG	Acoustic
resistance(Ω)	200G	100G	50 M	20GΩ	424.4M	100T
Area(mm^2)	TBD	4× 4 μm^2	132× 84.7 μm^2	0.071	0.075(total)	N/A
THD@-1dBFS	-113dB	-40dB	N/A	-74dB	N/A	N/A
Bandwidth(Hz)	20-20k	0.025-7.2k	5k	200-20k	75	20-4k
Output RMS noise contribution (μVrms)	2	207.7	151.2	140	N/A	178.4
SNR(dB)	96	60.6	30.6	66	N/A	67.5

I TBD = To be decided

II SCR = Switched-capacitor resistor

Ⅲ ACCA = AC-coupled amplifier

Rf-TIA = Resistor feedback transimpedance amplifier

Ⅳ ECG = Electrocardiogram

1.4 Thesis organization

This thesis explores a method for designing a 200 GΩ equivalent resistor for AC-coupled amplifiers in audio applications. The subsequent chapters are organized as follows:

Chapter 2 explores the feasibility of four different methods for this project, including duty-cycled resistors, switched-capacitor resistors, pseudo-resistors, and the active current reducer. Ultimately, an active cascade current reducer is chosen and applied to this project with circuit implementation details.

Chapter 3 showcases the simulation results.

Chapter 4 concludes this thesis with a discussion of future improvements.

Chapter 2 System architecture

This chapter discusses the system-level design of high-resistance resistor implementations for ACCA in audio applications. First, three distinct methods will be analyzed individually: duty-cycled resistors, switched-capacitor resistors, and pseudo resistors. Then, an architecture of the active current reducer will be introduced, and the system specification will be derived for the circuit-level design.

2.1 Analysis of high-resistance resistor implements

To explore the implementation of realizing a 200GΩ resistor in audio applications, we explore the following methods:

2.1.1 Duty-cycled resistor

A duty-cycled resistor, depicted in Figure 2.1, consists of a passive poly resistor in series with a switch. The basic idea of a duty-cycled resistor is to control the average current passing through the resistor within each cycle to achieve an equivalent high-resistance resistor. When a clock drives the switch with a duty cycle factor of D, the average resistance observed across the terminals is given by R/D.

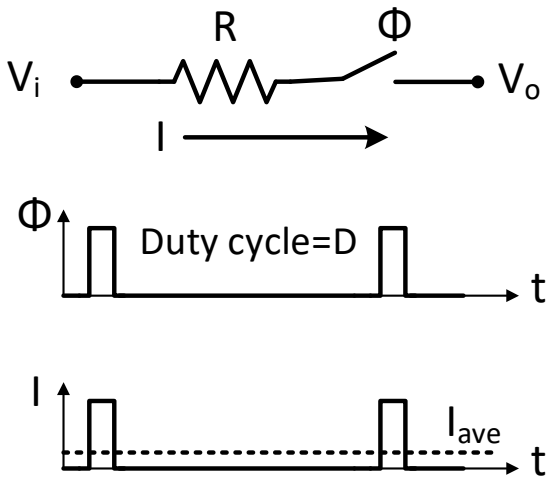

Figure 2.1 Concept of a duty-cycled resistor to realize a high-resistance resistance

Duty-cycled resistors are inherently time-varying. A more detailed analysis needs to account for frequency translations. Linear periodic time-varying (LPTV) analysis has been proposed in reference[15]. The frequency domain conductance of the duty-cycled resistor can be expressed as (2.1)

$$G(j\omega) = \sum_{k=-\infty}^{\infty} g_k \delta(\omega - k\omega_0) \tag{2.1}$$

Where $g_0 = \frac{D}{R}$ and $g_k = \frac{D}{R}\frac{\sin k\pi D}{k\pi D}$. When the duty-cycled resistor is incorporated into the AC-coupled amplifier, as illustrated in Figure 2.2(a), its noise model can be simplified into an equivalent noise model of a first-order RC low-pass filter, as shown in Figure 2.2(b). As mentioned in reference [14], the output RMS noise can be expressed by the following equation (2.2)

$$V_{n,out,rms} \cong \sqrt{\int_{20}^{20k} \frac{4kT\frac{R}{D}}{\left|1 + j2\pi f C_{fb}\frac{R}{D}\right|^2} df} \qquad (2.2)$$

From this equation, we can see that the noise transfer process for duty-cycled resistors is approximately the same as that of a poly resistor with an equivalent resistance value in ACCA. For a 200GΩ duty-cycled resistor achieved by ideal components, the output RMS noise measured is 31.6μV. The noise power spectral density of this structure is depicted in Figure 2.2(c). We can see that the noise behavior of the duty-cycled resistor is similar to that of the poly resistor. Using a duty-cycled resistor to implement a 200GΩ equivalent resistor does not meet the design goal of low noise.

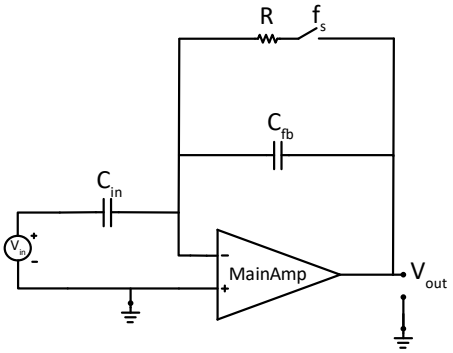

(a)

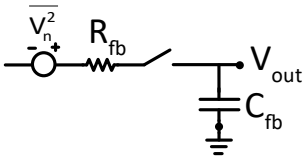

(b)

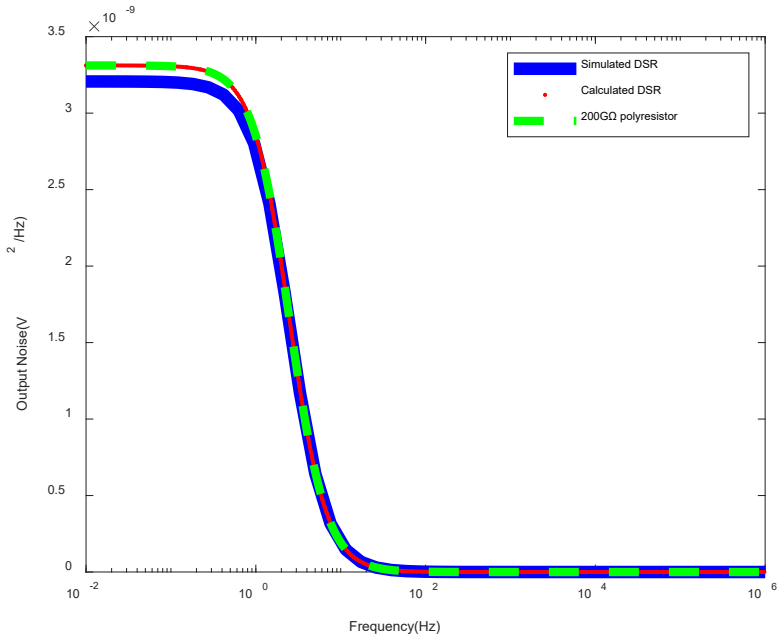

(c)

Figure 2.2 (a)ACCA with duty-cycled resistor; (b) Simplified noise model; (c) Noise power spectrum.

In terms of the implementation of the duty-cycled resistor, a complementary switch (Figure 2.3(a)) and a three-terminal poly resistor (3T-poly resistor, Figure 2.3(b)) are used to implement a duty-cycled resistor. Since the equivalent resistance is R/D, we investigate the smallest duty cycle to determine the highest achievable resistance using this structure. The switching frequency (40 kHz) is twice the audio bandwidth, satisfying the Nyquist criterion for a sampling system. Due to the parasitic capacitor to ground (mainly from on-chip resistors), the switching frequency forms a switched capacitor resistor with a resistance value of $1/C_p f$.

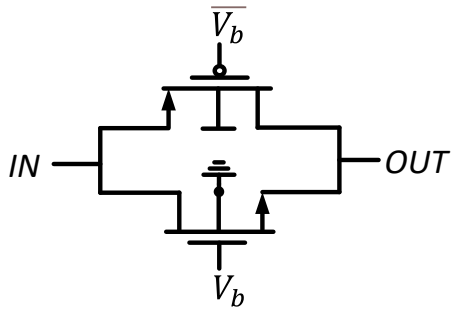

Figure 2.3 Complementary switch

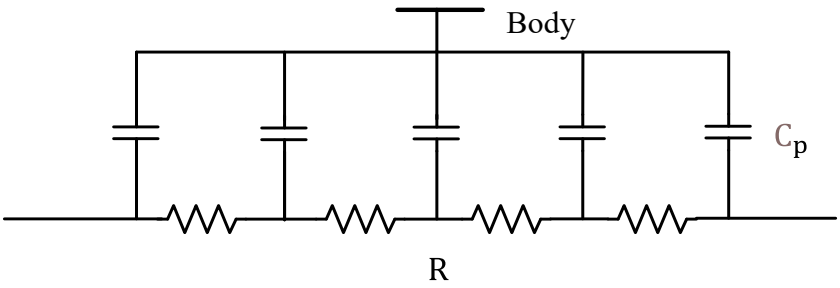

Figure 2.4 3T-poly resistor model

The formed switched-capacitor resistor is in parallel with the duty-cycled resistor. The final resistance value primarily depends on the smaller of the two resistors. To explore the influence of the parasitic distributed capacitance of the 3T poly resistor on the achievable resistance value, we use different 3T poly resistors to make a duty-cycled resistor. The results are shown in Table 2.1. We can see that the attainable resistance value is limited by the switch parasitic capacitor resistor, which has a proportional relationship with the size of the resistor. To achieve a 200GΩ equivalent resistance, we need a 50kΩ resistor with a duty cycle of 1/4000000. The feasibility of implementing such a small duty cycle warrants further investigation.

Table 2.1 Achievable resistance by different 3-T poly resistor

R(Ω)	50k	100k	1M	10M
D	1/4M	1/2M	1/200k	1/20k
C_p(F)	0.128f	0.256f	2.57f	25.7f
Achievable resistance	200G	97.6G	9.7G	0.97G

We explored the feasibility of implementing such a small duty cycle , which depends on the pulse width. Figure 2.6 illustrates a simple pulse width generator consisting of a clock signal, an inverter, and an AND gate. The delay of the inverter determines the pulse width of the pulse width generator. As demonstrated in Figure 2.6, we obtained a 0.4 ns delay, where the PNMOS inverter exhibits a delay of approximately 0.4 ns compared to an ideal inverter. The minimum achievable duty cycle for a 40 kHz switching frequency is 1/62,500.

Consequently, the maximum resistance value attainable with this structure is 3 GΩ. In a recent paper [26], it has been claimed that a pulse width of 16ps has been achieved in 14nm technology. However, even with such a small pulse width, the maximum achievable resistance is 100 GΩ, which remains insufficient to meet the 200 GΩ target.

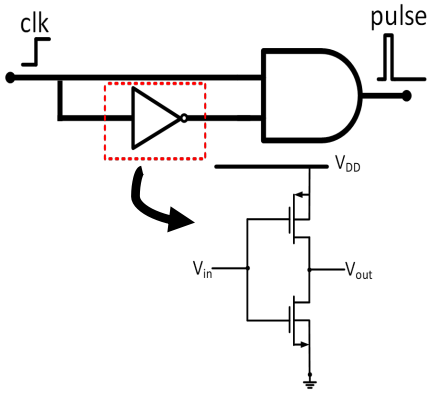

Figure 2.5 Pulse width generator

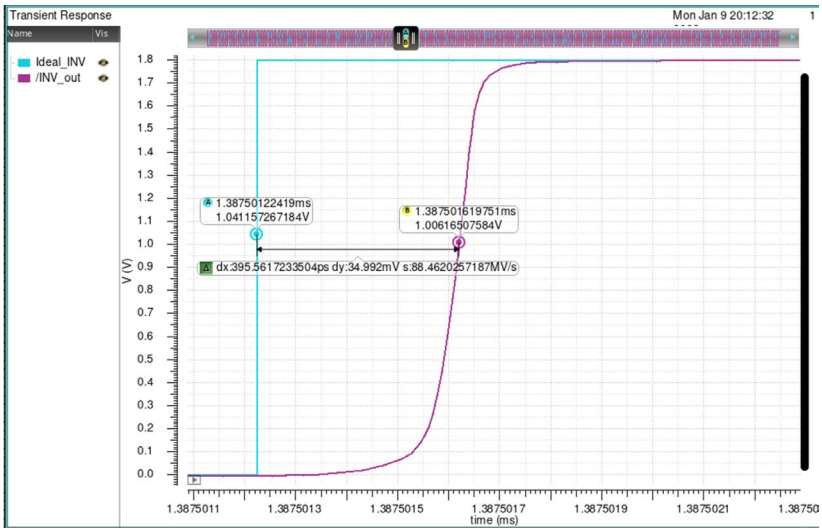

Figure 2.6 Transient response of ideal inverter (blue line) and push-pull PNMOS inverter (purple line)

In summary, a duty-cycled resistor provides an area-efficient method for achieving substantial resistance. However, its maximum value is constrained by parasitic capacitors, switching frequency, and duty cycle.

Due to the abovementioned limitations, the duty-cycled resistor was not chosen for this project. Nevertheless, several approaches have been proposed to enhance performance, such as sample and average feedback structures [27]. By constructing an anti-aliasing filter, the switching frequency of the DSR can be further reduced without introducing aliasing, which helps to achieve a higher resistance value. Recently, a segmented duty-cycled resistor structure [28] has been proposed, which realizes TΩ resistance by connecting multiple duty-cycled resistors. In each cycle, parasitic capacitors share charge, mitigating the restrictions on achievable resistance. Future work will further explore the potential of DSR in audio applications by examining these methods.

2.1.2 Switched-capacitor resistor

The switched-capacitor resistor, illustrated in Figure 2.7, comprises two switches and one capacitor. The basic principle is controlling the charging and discharging rates of the capacitor by switches to achieve a small resistance. The resistance value of the switched-capacitor resistor can be expressed as $\frac{1}{Cf_s}$ [29].

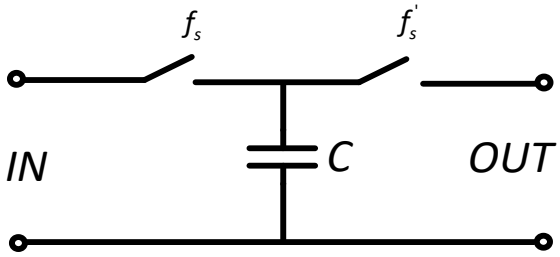

Figure 2.7 Switched-capacitor resistor

When this resistor is placed in ACCA, as shown in Figure 2.8(a), its noise contribution model can be simplified into an equivalent noise model of a first-order RC low-pass filter, as demonstrated in Figure 2.8(b). based on the methods mentioned in [20][30][31], the output RMS noise from the equivalent resistor can be represented by the following equation (2.3).

$$V_{n,out,rms} \simeq \sqrt{\int_{20}^{20k} \frac{4kT\frac{1}{C_c f_s}}{\left|1 + j2\pi f C_{fb}\frac{1}{C_c f_s}\right|^2} df} \tag{2.3}$$

For the switched-capacitor resistor, its noise transfer process is approximately equivalent to that of a poly resistor with the same resistance value in ACCA. For a 200 GΩ switched-capacitor resistor implemented with ideal components, the measured output RMS noise is 33μV, and its noise spectral density is shown in Figure 2.8(c). As seen in the figure, the noise curve of the switched-capacitor resistor closely aligns with the noise curve of the poly resistor, consistent with the description provided by the noise formula. A 200 GΩ equivalent switched-capacitor resistor does not meet the necessary noise requirements.

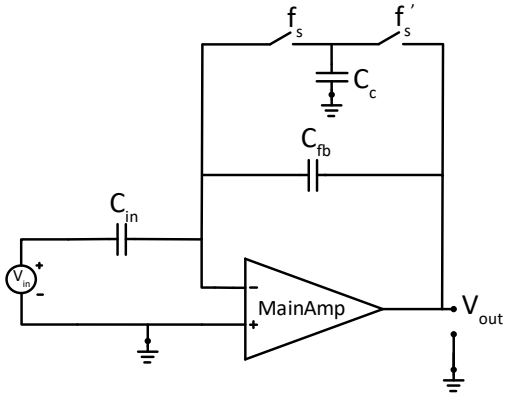

(a)

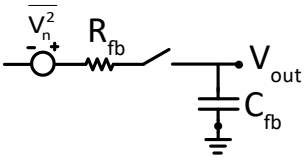

(b)

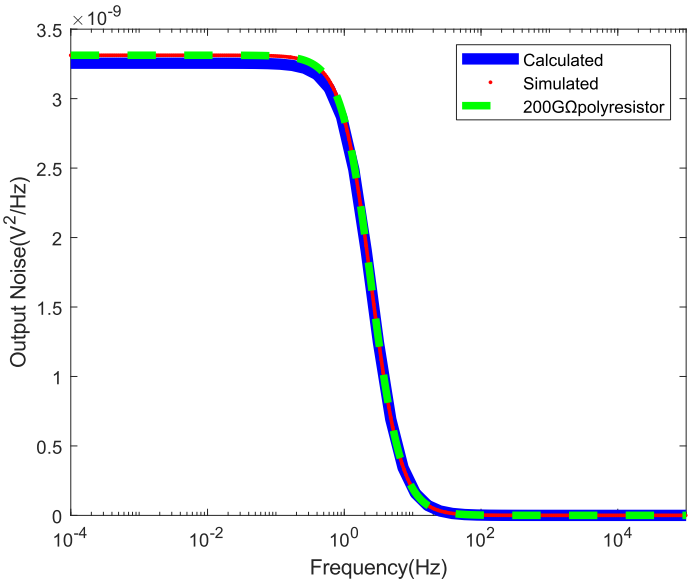

(c)

Figure 2.8 (a)ACCA with switched-capacitor resistor; (b) Simplified noise model; (c) Noise power spectrum.

In terms of implementation, a switched-capacitor resistor comprises a pair of non-overlapping complementary switches and a capacitor, as shown in Figure 2.9. Given that the equivalent resistance is inversely proportional to both the switching frequency and capacitance, the switching frequency is set to 40 kHz based on the Nyquist theorem to investigate the maximum achievable resistance. A 0.125fF capacitor is needed to achieve 200G equivalent resistance. For making such a small capacitance, we explore the feasibility.

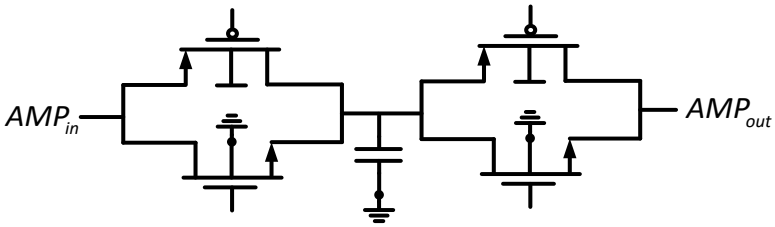

Figure 2.9 non-overlapping complementary switches

In the 180-nm BCD process, the minimum capacitance value is 6.23 fF by a CRTMOM capacitor component. To achieve a smaller capacitance value, two methods are proposed. The first method involves connecting multiple capacitors in series. However, the presence of parasitic capacitance to the ground constrains the minimum capacitance that can be attained. To measure this parasitic capacitance, a capacitor is grounded in the layout, as illustrated in Figure 2.10. The measured parasitic capacitance to the ground is found to be 0.33 fF.

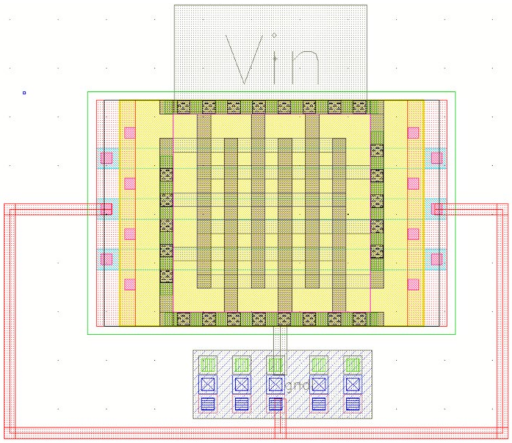

Figure 2.10 Layout for a parasitic capacitor connected to the ground

The minimum achievable capacitance can be determined using the mean inequality equation (2.4).

$$\frac{6.2}{x} + 0.33x \geq 2.8\text{fF} \tag{2.4}$$

The left-hand side of the inequality comprises two components. The first component is the capacitance obtained by connecting capacitors in series, where theoretically, the more capacitors connected, the smaller the total capacitance value. The second component is the parasitic capacitance to the ground, which increases as the number of capacitors in the series grows since the parasitic capacitors are connected in parallel. Figure 2.11 presents the results of a Monte Carlo simulation involving nine capacitors in series, yielding a capacitance of 2.65 fF, closely approximating the theoretical value. Consequently, achieving such a small capacitance with capacitors in series is not feasible under the 180-nm BCD process.

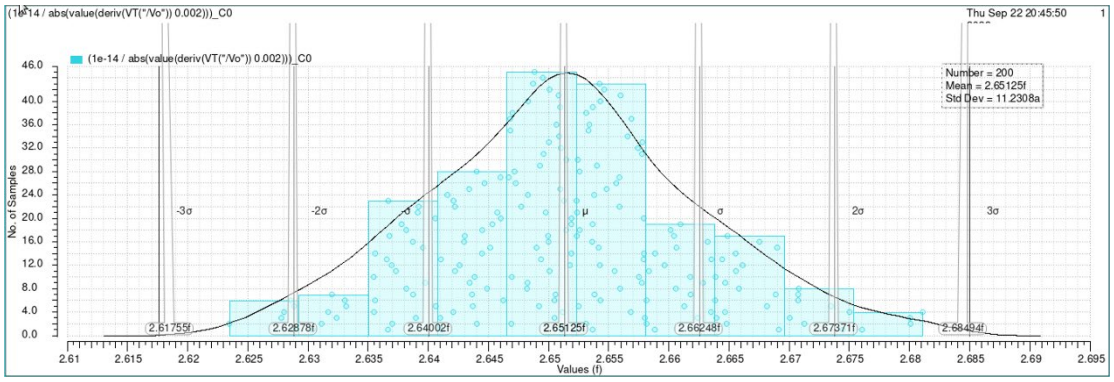

Figure 2.11 Monte Carlo simulation results of capacitors in series

An alternative approach to attaining a small capacitance involves using two metal plates. Figure 2.12 depicts the overlapping contacts of two poly resistors, which result in a metal capacitor with a capacitance of 0.125 fF in the Cadence simulator by adjusting the contact area. Paper [32] also achieved a minimum capacitor of 0.125fF in the 65-nm BCD process. However, achieving and ensuring the reliability of such a small metal capacitance in a 180-nm BCD process remains challenging and requires

further investigation and validation.

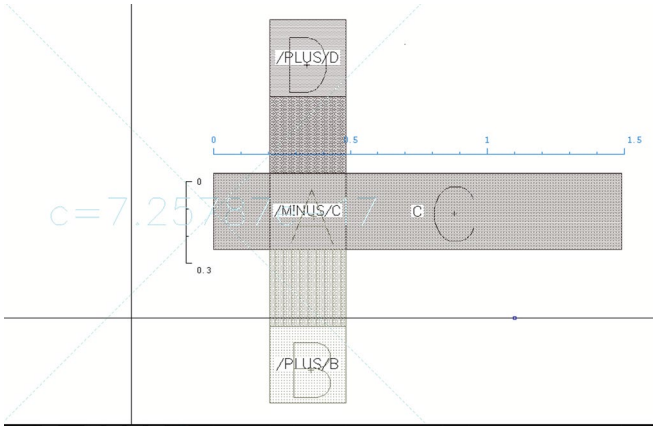

Figure 2.12 Metal capacitor made by contact of two poly resistor

This project did not choose switched-capacitor resistors (SCR) due to the aforementioned problems. The sample and average feedback structure proposed in [27] could increase capacitance and reduce switching frequency without introducing aliasing, thereby facilitating higher resistance. Future work will focus on implementing a small capacitor and lowering the switching frequency to assess the feasibility of SCR in audio applications.

2.1.3 Pseudo resistor

Pseudo resistors (PRs) are widely used in biomedical readout ICs. PRs provide high resistance within the acceptable chip consumption area. A diode-connected PMOS is the simplest way to make a pseudo resistor, as shown in Figure 1.13 (a). Typically, PRs are biased in the sub-threshold region to minimize current, but the linearity is limited by the nonlinear of weak inversion MOSFETs [33]. Figure 1.13 (b) illustrates that the pseudo resistor exhibits different conduction modes for different voltage signals, resulting in an asymmetric voltage-current relationship. This relationship contributes to the nonlinearity of the pseudo resistor structure. When a 200G Ω pseudo resistor is placed in an ACCA (Figure 1.13 (c)), the THD at -1dBFS is only -16.5dB, which is far from the requirements for audio applications. The linearity of the pseudo resistor can be enhanced by implementing a back-to-back structure, as depicted in Figure 1.13 (d). This symmetrical arrangement reduces even harmonic distortion and improves the linearity of the overall structure [12]. Although the THD increases to -31dB, it remains unsuitable for audio applications.

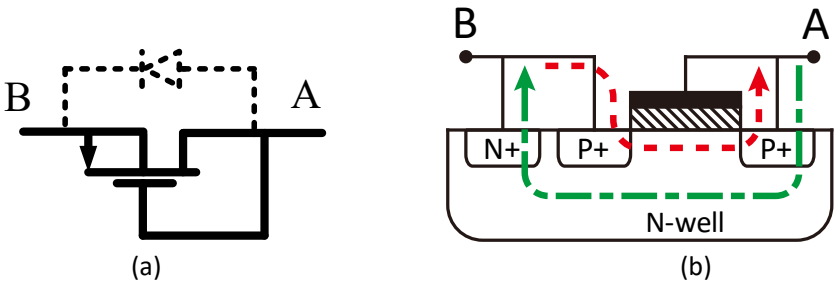

(a) (b)

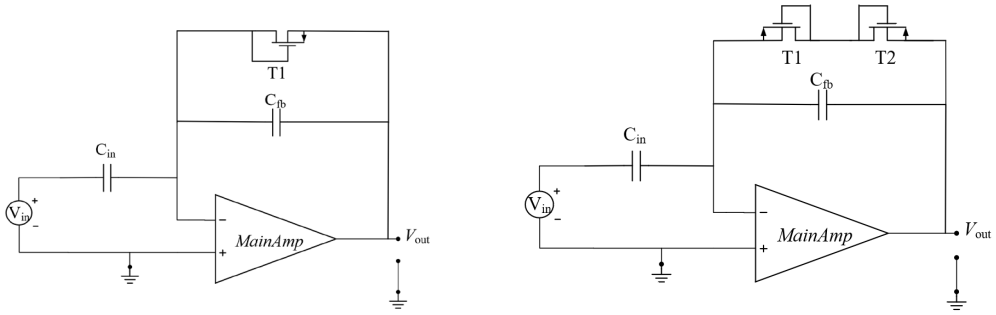

(b) (d)

Figure 2.13 (a) Diode connected PMOS as pseudo resistor; (b) Cross-section of the pseudo resistor; (c) A pseudo resistor in ACCA; (d) Back-to-back pseudo resistor in ACCA

The noise and resistance of pseudo resistors are highly sensitive to process and temperature variation due to the change in charge carrier mobility [34]. For instance, a 200GΩ pseudo resistor at room temperature exhibits significant resistance and noise contribution fluctuations at different temperatures and process corners, as illustrated in Table 2.1. It is important to note that a 200GΩ pseudo resistor generates less noise than other resistors with equivalent resistance, as previously mentioned. A preliminary explanation for this phenomenon is that the noise of the pseudo resistor does not adhere to the 4kTR formula when operating in weak inversion. In this project, the pseudo resistor has a zero bias and functions in the off region, resulting in considerably lower noise levels than other resistors with the same resistance value. Further investigation and validation of this observation will be conducted in future work. The lower noise performance of pseudo resistors offers the potential to meet low-noise requirements, which we will use in the following.

Table 2.1 Resistance and noise contribution over temperature and process corner

Process corner	RMS noise 0°C	RMS noise 27°C	RMS noise 150°C	R_{DC} 0°C	R_{DC} 27°C	R_{DC} 150°C
TT	500nV	3.25µV	125.1µV	1.2TΩ	200GΩ	927.6MΩ
SS	64nV	515nV	97µV	8.17TΩ	1.08TΩ	2.7GΩ
FF	4.95µV	24µV	133.3µV	144GΩ	27.37GΩ	218.7MΩ

In summary, pseudo resistors offer an area-efficient method for achieving high equivalent resistance. However, their nonlinearity and sensitivity to process corner and temperature variations limit their application in audio systems. For more information about pseudo resistors, refer to [12].

An active resistor structure (Figure 2.14) called the active current reducer (ACR) [25] could help with low linearity and high sensitivity for process corner and temperature variation of the pseudo resistor. The basic idea of this structure is to use matched pseudo-resistors T_1 and T_2 with equal channel length and bias voltage but different multipliers, ensuring consistent current density in each PMOS. The multiplier of T_2 is designed to be M times larger than T1, enabling the system to work as a linear and

precise current attenuator, dividing the current converted from R_{att} by a factor of M. This structure converts the output voltage into a reduced current, achieveing an equivalent resistance of $M*R_{att}$.

The output noise of the active current reducer is primarily composed of two parts: thermal noise from the physical resistor R_{att} and the noise from the pseudo-resistance T_1. For thermal noise from R_{att}, the current thermal noise is reduced by a factor of M^2. the pseudo resistor T1 operates at zero DC bias in ACCA. Although there is no definitive noise model for pseudo resistors, Table 1.2 indicates that their noise contribution to the output is inversely proportional to their equivalent resistance value. In order to explore the possibility of ACR achieving the noise requirement, the smallest aspect of T1 has been applied, which minimizes the current noise from T1. By increasing the multipliers, M, to reduce the noise contribution from R_{att} with the same equivalent resistance, the output RMS noise (Figure 2.15) will be dominated by T_1. As shown in the chart, the minimum output noise achieved by this structure remains far from our noise requirements.

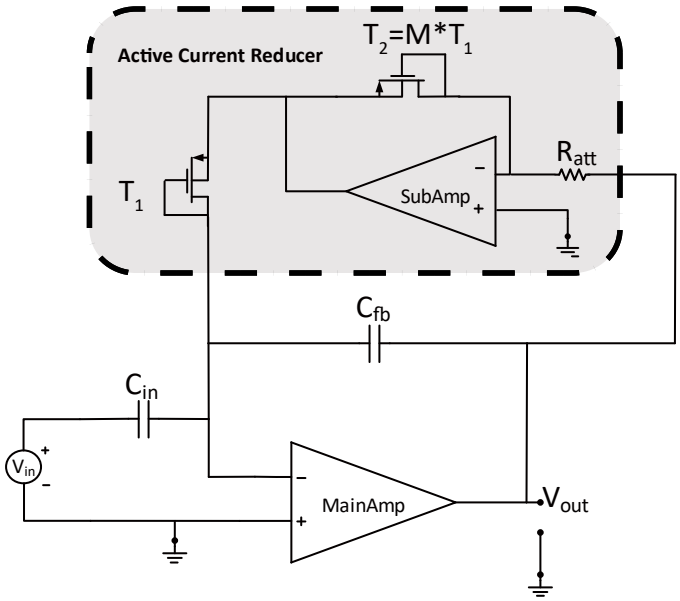

Figure 2.14 ACCA with active current reducer

Furthermore, this structure needs a large number of transistors to achieve a high equivalent resistance. For example, using a 10M Ω physic resistor would require 20001 pseudo resistors to achieve 200GΩ, which consumes a large amount of chip area.

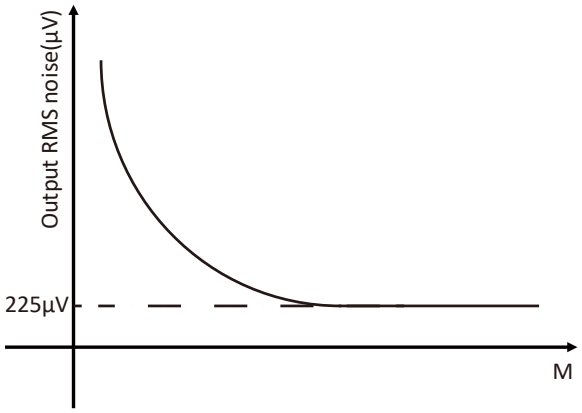

Figure 2.15 Output RMS noise of ACCA with ACR

To reduce noise and decrease the area consumption by pseudo resistors, we use cascade active current reducers(CACR), as shown in Figure 2.16. The equivalent resistance for CACR is $M_1 \times M_2 \times R_{att}$, and the number of pseudo resistors is $M_1 + M_2$ compared with M1 × M2 for ACR structure.

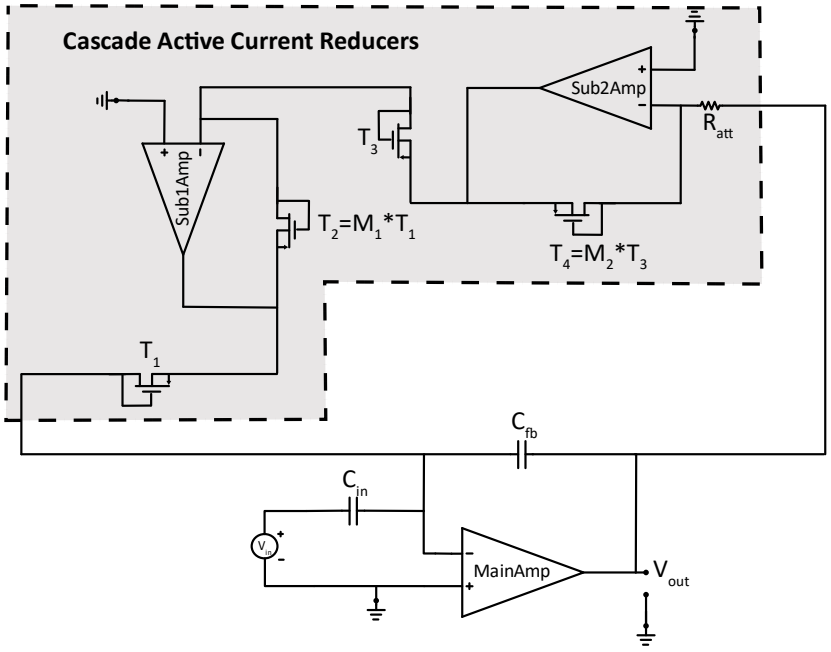

Figure 2.16 ACCA with cascade active current reducers

The pseudo resistors T_3 and T_4 are made of low-voltage PMOS, while the pseudo resistors T_1 and T_2 are made of high-voltage PMOS. This kind of design allows the input noise of the CACR structure (the output noise of ACCA) to be suppressed by CACR's closed-loop gain, and the pseudo resistor made of high voltage PMOS could achieve a higher impedance to reduce the noise of the structure further. By balancing the number of transistors and the output noise, R_{att} (5.8 MΩ), M_1 (138), and M_2 (250) are chosen where the structure achieves an output RMS noise of 2μV in the worst-case, as shown in Figure 2.17. The noise is contributed from T_3 and T_1. The noise contribution

from T_3 could be decreased by increasing the number of pseudo resistors, further lowering the overall noise.

Device	Param	Noise Contribution	% Of Total
/T3	id	1.63005e-06	65.82
/T1	id	1.14773e-06	32.63
Ratt.rmain	thermal_noise	2.05257e-07	1.04
/T4	id	1.03093e-07	0.26
/T2	id	9.77009e-08	0.24
/T3	rd	2.28374e-09	0.00

Integrated Noise Summary (in V) Sorted By Noise Contributors
Total Summarized Noise = 2.00914e-06
Total Input Referred Noise = 2.51868e-07
The above noise summary info is for noise data

Figure 2.17 Noise summary of output RMS noise for ACCA with CACR at worst case

Cascade active current reducers incorporate amplifiers, and the linearity of the equivalent resistor is related to the amplifier's gain. The relationship between the equivalent resistance and the amplifier's gain can be derived through Kirchhoff's Voltage Law (KVL) as the Equation (2.5).

$$R_{eq} = \frac{R_{T3}}{R_{T4}} \times \frac{R_{T1}}{R_{T2}} \times R_{att} \times \left(1 + \frac{1}{A_{sub2}} + \frac{R_{T4}}{R_{att}} \frac{1}{A_{sub2}}\right) \times \left(1 + \frac{1}{A_{sub1}} + \frac{R_{T2}}{R_{T3}} \frac{1}{A_{sub1}}\right) \quad (2.5)$$

The formula demonstrates that, for an ideal amplifier, the equivalent resistance of CACR equals $M_1 \times M_2 \times R_{att}$. The nonlinearity of the pseudo resistor will be introduced to the structure when the amplifier's gain decreases, which is also the same for the bandwidth. Figure 2.18(a)(b) shows the effect of different gains and bandwidths on the THD. It is evident that a decrease in gain and bandwidth reduces the linearity of the resistor. To meet the linearity requirement, the gain and bandwidth for Sub-Amp 1 are set to 8k and 400 Hz, while those for Sub-Amp 2 are chosen as 5k and 120 Hz, respectively.

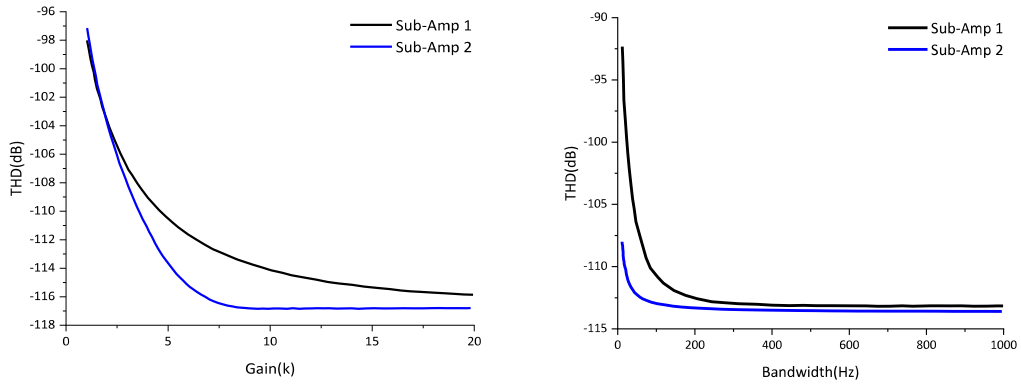

(a) (b)

Figure 2.18 (a) Gain of sub-amplifiers for the THD; (b) 3db-bandwidth of sub-amplifiers for the THD

The noise of the amplifier also contributes noise to the output. R_{sub1} and R_{sub2} serve as equivalent noise resistors, representing the amplifier's noise within the noise transfer process, as shown in Figure 2.19(a)(b).

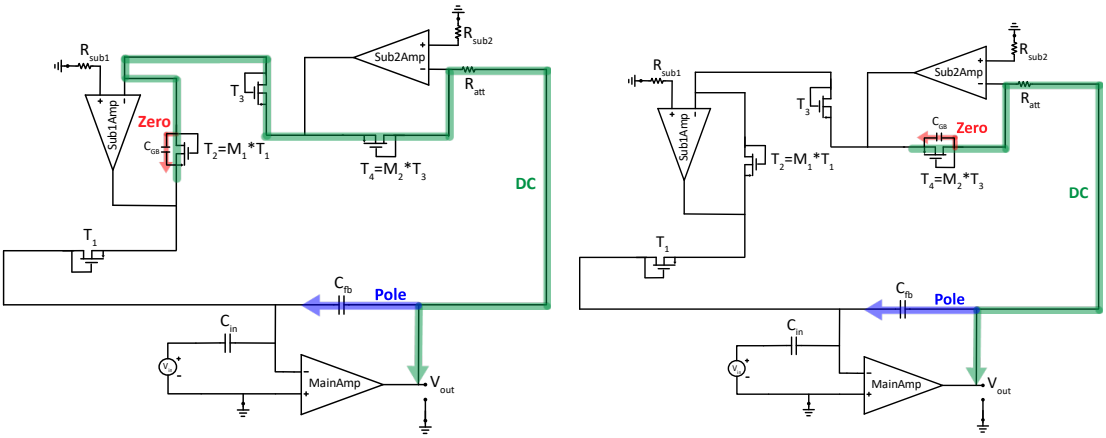

Figure 2.19 (a) Noise transfer process of sub1-amplifier; (b) Noise transfer process of sub2-amplifier

The noise transfer function (NTF) of R_{sub1} and R_{sub2} can be represented by KVL as Equation (2.6)

$$\begin{aligned} NFT_{Rsub1} &= (1+\frac{R_{T3}}{R_{T2}})\times\frac{R_{att}}{R_{T4}}\times\frac{1+s(R_{T2}\,||\,R_{T3})C_{gb\_T2}}{1+sR_{fb}C_{fb}} \\ NFT_{Rsub2} &= (1+\frac{R_{att}}{R_{T4}})\times\frac{1+s(R_{att}\,||\,R_{T4})C_{gb\_T4}}{1+sR_{fb}C_{fb}} \end{aligned} \tag{2.6}$$

The NTF reveals that the feedback resistor and feedback capacitor contribute to the pole, while the parasitic capacitor of the pseudo resistor contributes to the zero. By selecting the equivalent noise resistors of the R_{sub1} and R_{sub2} to 3kΩ and 30MΩ, respectively, their output RMS noise contribution to the output is 0.67μV (14% of 2μV), which can be negligible. The SNR is 96.7dB, and after applying and after applying the A-weighting filter, the A-weighted SNR is 97.9 dB, as seen in Figure 2.20.

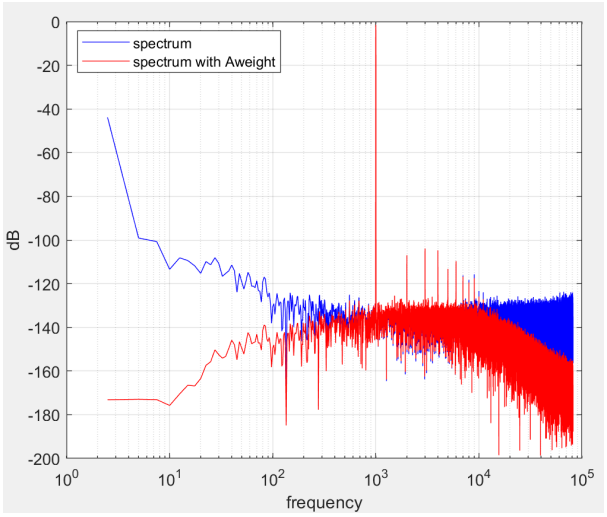

Figure 2.20 Frequency spectrum before and after A-weighting filter

The CACR structure achieves a high equivalent resistance with the required linearity and noise performance. This structure is chosen for application in this project.

2.2 The circuit blocks of the main amplifier

The topology of the main amplifier is based on a previously established structure [2]. A two-stage amplifier with Miller compensation is applied, as shown in Figure 2.21.

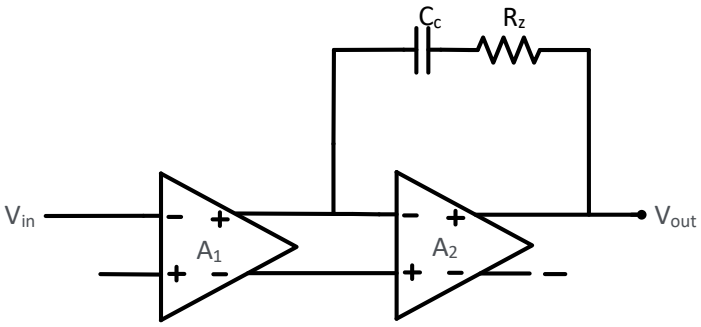

Figure 2.21 a two-stage amplifier with miller compensation

The first stage amplifier uses a cascode amplifier with source degeneration, as shown in Figure 2.22. The PMOS input and source degeneration reduce the flicker noise compared with the NMOS input cascode stage.

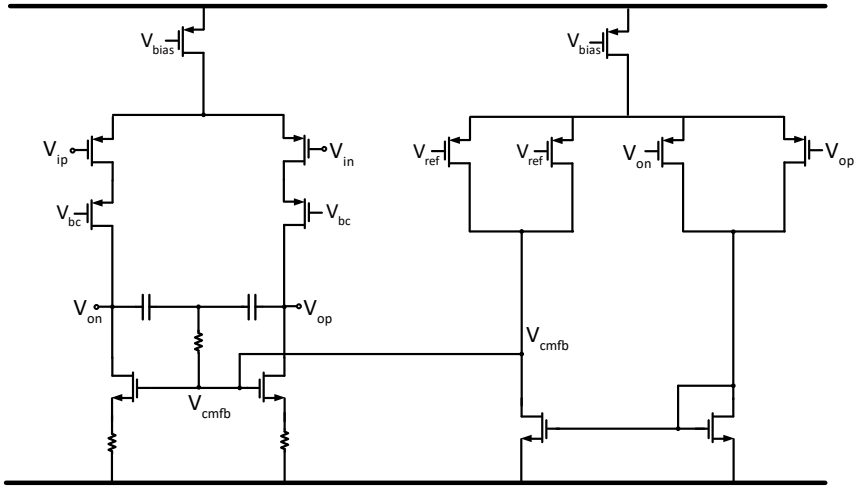

Figure 2.22 Cascode amplifier with source degeneration

The second stage amplifier uses an inverter input amplifier to achieve a larger scale output swing than a cascode stage, as shown in Figure 2.23

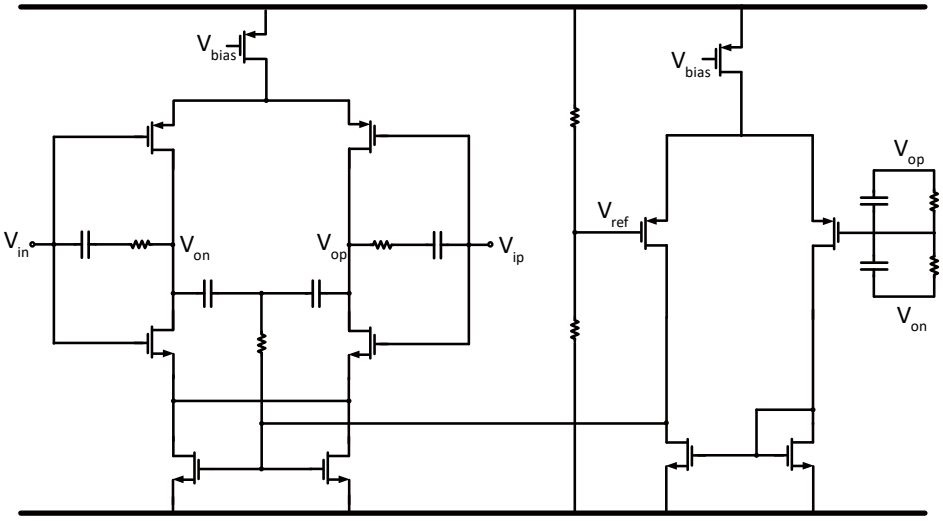

Figure 2.23 Inverter input amplifier

2.3 Conclusion

This chapter concentrates on various methods to implement high-resistance resistors. We have conducted behavioral simulations for feasibility verification. CACR, a way to achieve a high resistance, which meets the requirements for linearity and noise contribution, has been applied to ACCA for audio applications. The next chapter will discuss the simulation results and analysis of the whole circuit with the CACR at different temperatures and process corners.

Chapter 3 Simulation results

In this chapter, the simulation results will be presented and analyzed. We will cover the following topics in turn: resistance, noise contribution, and linearity. Finally, a comparison with other designs will be made. The whole circuit is built in a 180-nm BCD process. The output stage employs a 1.8V voltage supply.

3.1 Resistance variation

Table 3.1 shows the resistance variation of CACR at different temperatures and process corners. For a 200GΩ equivalent resistor, the resistance fluctuates within the range of 174.6GΩ to 234GΩ (± 20%), which is within an acceptable range. This fluctuation mainly comes from the physical resistor R_{att} whose resistance changes by temperature and process corner. The measurement results also indicate that a well-matched MOS structure in the ACR compensates for the temperature and process sensitivity issues related to pseudo resistors.

Table 3.1 Resistance variation measurement results

Process corner	TT	SS	SF	FF	FS
Resistance (0°C)	203 GΩ	234 GΩ	201 GΩ	179 GΩ	217 GΩ
Resistance (27°C)	200 GΩ	221 GΩ	200 GΩ	178 GΩ	201 GΩ
Resistance (150°C)	196 GΩ	217 GΩ	196 GΩ	175 GΩ	196 GΩ

3.2 Noise variation

Table 3.2 presents the output RMS noise contribution of the equivalent resistance under varying temperatures and process corners. The best-case noise is 80 nV, and the worst-case is 2.1 μV. The output RMS noise variation mainly results from the noise

change of the pseudo resistor T1 at the output of the CACR, which is affected by different process corners and temperatures. Even in the worst case, the structure meets noise requirements due to the closed-loop gain of the two-stage sub-amplifier and the high-voltage PMOS's low-noise performance.

Table 3.2 Noise variation measurement results

Process corner	TT	SS	SF	FF	FS
RMS noise (0°C)	96 nV	80 nV	96 nV	119 nV	96 nV
RMS noise (27°C)	100 nV	83 nV	101 nV	125 nV	101 nV
RMS noise (150°C)	303 nV	121 nV	1.3 μV	2.1 μV	135 nV

3.3 Linearity variation

Linearity performance simulations use a 1kHz, -1dBFS input, and 4-Ω load. Figure 3.1 illustrates the output spectrum and time-domain waveform across temperature and process corners. The THD ranges from -106 dB to -116 dB. The worst THD is -106dB, which is lower than the design requirement but still acceptable for audio applications. THD variation arises from the limited gain and bandwidth of sub-amplifiers in CACR, which cannot adequately suppress the nonlinearity of the pseudo resistor. Enhancing the gain and bandwidth of sub-amplifiers within the CACR could further optimize the system's linearity performance. Due to the feedback capacitor's nonlinearity, the best THD at the output is limited to -116dB.

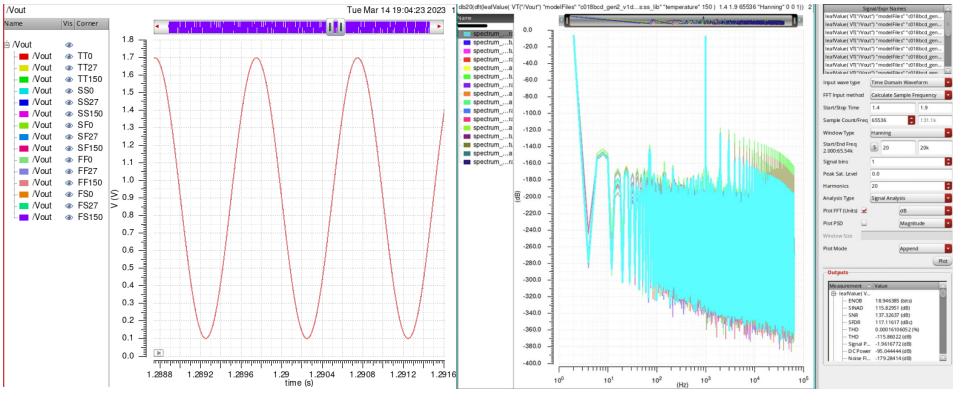

Figure 3.1 The spectra and waveforms

3.4 Comparison with other designs

A performance summary of ACCA with CACR and a comparison with the state-of-the-art are shown in Table 3.3 below.

This work achieves a 200GΩ equivalent resistance for ACCA with a 2.1μV output RMS noise contribution and a worst-case THD of -106dB, making it suitable for audio applications. The THD is primarily limited by the gain and bandwidth of amplifiers and can be improved in future work. The presented design demonstrates competitive SNR and linearity compared to state-of-the-art solutions.

Table 3.3 Comparison with the state of the art

	This Work	03-JSSC[8]	12-Sensors and Actuators[9]	17-JSSC[14]	20-Centurelli [16]	21-VLSI [21]
Resistor Structure	CACR [I]	pseudo resistor	pseudo resistor	Duty-cycled resistor	Duty-cycled resistor	SCR [II]
Architecture [III]	ACCA	ACCA	Rf-TIA	Integrator	RC-filter	ACCA
Application [IV]	Audio application	ECG	DNA	ECG	ECG	Acoustic
resistance(Ω)	200G	100G	50 M	20GΩ	424.4M	100T
Area(mm^2)	0.003	4× 4 μm^2	132× 84.7 μm^2	0.071	0.075(total)	N/A
THD@-1dBFS	-106dB	-40dB	N/A	-74dB	N/A	N/A
Bandwidth(Hz)	20-20k	0.025-7.2k	5k	200-20k	75	20-4k
Output RMS noise contribution (μVrms)	2.1	207.7	151.2	140	N/A	178.4

SNR(dB)	96.7	60.6	30.6	66	N/A	67.5

Ⅰ CACR = cascode active current reducer

Ⅱ SCR = Switched-capacitor resistor

Ⅲ ACCA = AC-coupled amplifier

Rf-TIA = Resistor feedback transimpedance amplifiers

Ⅳ ECG = Electrocardiogram

Chapter 4 Conclusions

4.1 Thesis contribution

This work contributes to audio applications by offering a solution for achieving high resistances with low noise and high linearity. A cascade active current reducer (CACR) has been proposed in this thesis to obtain a high equivalent resistance resistor and low cut-off frequency in ACCA with low noise contribution and high linearity. The CACR structure performs 200GΩ with 0.003 mm^2 area consumption and ± 20% resistance variation. The resistor contributes 2.1μV RMS noise to the output and results in -106dB THD in the ACCA for a bandwidth range from 20Hz to 20kHz, meeting the SNR and THD requirements for audio applications. Compared to existing research, this work accomplishes lower noise and better linearity in implementing high-resistance resistors for ACCA in audio applications.

This thesis presents different methods of making high equivalent resistance resistors for ACCA in audio applications. Different methods such as DSR, SCR, pseudo resistor, and active current reducer are explored to explore the possibilities of high-resistance resistors in audio applications, along with analysis and discussion about the implementation of equivalent resistance, noise performance, and resistor characteristics.

This project combines high-resistance, low-noise pseudo resistors with current reducers to achieve high resistance, low noise, high linearity, and temperature and process corners robustness. The CACR was chosen and optimized for audio applications. The thesis also suggests possibilities and methods for further optimization of other resistor structures.

4.2 Future work

The proposed active current reducer structure meets most design requirements and provides a solution for high-resistance resistors in audio applications. However, several steps are necessary to develop a practical demonstrator:

1. The THD could not fully meet the design requirements. Further optimization of the amplifier is needed to improve linearity performance.

2. The noise performance of pseudo resistors requires further exploration and validation. Pseudo resistors offer lower noise than physical resistors with the same resistance value in simulations, which needs to be verified and further explored

through tape-out and measurement. A detailed noise and linearity model for pseudo resistors must be established to design and optimize CACR.

3. Based on the previous design, the main amplifier contributes most of the noise. A new amplifier should be designed for high-resistance resistor feedback ACCA to achieve lower noise.

4. The current resistance value is somewhat arbitrarily chosen. The ACCA circuit and acoustic design should be considered for optimized resistance value selection.

This project has explored other methods of implementing high-resistance resistors. Although not chosen for this work, these methods may still be applied in ACCA for audio applications. Future research can explore these possibilities:

For duty-cycled resistors, anti-aliasing filters could be applied to achieve higher resistance values. Implementing smaller duty cycles could increase the achievable resistance value. Connecting multiple DCRs may also achieve higher resistance values.

For switched-capacitor resistors, anti-aliasing filters could help achieve higher resistance. In this thesis, a 0.125fF capacitor is created by the layout, but its reliability needs verification through tape-out and measurement. Exploring the implementation of smaller capacitors could improve achievable resistance values.

Noise suppression techniques can be applied to achieve low output noise contributions for high-resistance resistors.

Further exploration of methods for implementing equivalent high-resistance resistors, such as T-network resistors [35], could be valuable. Combining different methods to achieve high equivalent resistances is also a promising research direction.

Reference

[1] Texas Instruments, TPA3255-Q1 315-W Stereo, 600-W Mono PurePath™ Ultra-HD Analog-Input, [Online]. Available: https://www.ti.com/lit/gpn/tpa3255-q1

[2] H. Zhang et al., "A −109.1 dB/−98 dB THD/THD+N Chopper Class-D Amplifier with >83.7 dB PSRR Over the Entire Audio Band," ESSCIRC, pp. 1-2, Sept. 2021.

[3] Fan, Qinwen. "Capacitively-coupled chopper amplifiers." *Delft University of Technology. Ipskamp Druckkers BV* (2013).

[4] H. Zhang, M. Berkhout, K. A. A. Makinwa and Q. Fan, "A 121.4-dB DR Capacitively Coupled Chopper Class-D Audio Amplifier," in *IEEE Journal of Solid-State Circuits*, vol. 57, no. 12, pp. 3736-3745, Dec. 2022, doi: 10.1109/JSSC.2022.3207907.

[5] iLoud Precision 6 User Manual [Online].Available: https://download.ikmultimedia.com/plugins/Manuals/iLoudPrecision6/iLoud_Precision_6_User_Manual.pdf

[6] Genelec 8050B Studio Monitor Technical Specifications [Online].Available: https://www.genelec.com/8050b#section-technical-specifications

[7] ICEpower 700AS2 Datasheet [Online]. shifthttps://blackdotaudio.eu/upload/6186d535d0de76.79679237.pdf

[8] Harrison, R.R. and Charles, C., 2003. A low-power low-noise CMOS amplifier for neural recording applications. *IEEE Journal of solid-state circuits*, *38*(6), pp.958-965.

[9] Kim, J., Pedrotti, K. and Dunbar, W.B., 2013. An area-efficient low-noise CMOS DNA detection sensor for multichannel nanopore applications. *Sensors and Actuators B: Chemical*, *176*, pp.1051-1055.

[10] Hu, H., Islam, T., Kostyukova, A., Ha, S. and Gupta, S., 2018. From battery enabled to natural harvesting: Enzymatic biofuel cell assisted integrated analog front-end in 130nm CMOS for long-term monitoring. *IEEE Transactions on Circuits and Systems I: Regular Papers*, *66*(2), pp.534-545.

[11] Wang, S., Lopez, C.M., Ballini, M. and Van Helleputte, N., 2018. Leakage compensation scheme for ultra‐high‐resistance pseudo‐resistors in neural amplifiers. *Electronics Letters*, *54*(5), pp.270-272.

[12] Guglielmi, E., Toso, F., Zanetto, F., Sciortino, G., Mesri, A., Sampietro, M. and Ferrari, G., 2020. High-value tunable pseudo-resistors design. *IEEE Journal of Solid-State*

Circuits, *55*(8), pp.2094-2105.

[13] Kurahashi, P., 2010. *Duty-cycle controlled switched resistor techniques for continuously tunable, low-voltage circuits*. Oregon State University.

[14] Chandrakumar, H. and Marković, D., 2017. A high dynamic-range neural recording chopper amplifier for simultaneous neural recording and stimulation. *IEEE Journal of Solid-State Circuits*, *52*(3), pp.645-656.

[15] Chandrakumar, H., 2018. *Implantable Neural Recording Front-Ends for Closed-Loop Neuromodulation Systems*. University of California, Los Angeles.

[16] Centurelli, F., Fava, A., Monsurrò, P., Scotti, G., Tommasino, P. and Trifiletti, A., 2020. Low power switched-resistor band-pass filter for neural recording channels in 130nm CMOS. *Heliyon*, *6*(8), p.e04723.

[17] Centurelli, F., Fava, A., Scotti, G. and Trifiletti, A., 2021. A Detailed Model of the Switched-Resistor Technique. *IEEE Open Journal of Circuits and Systems*, *2*, pp.497-507.

[18] Rothe, R., Cho, M., Choo, K., Jeong, S., Sylvester, D. and Blaauw, D., 2021, June. A 192 nW 0.02 Hz high pass corner acoustic analog front-end with automatic saturation detection and recovery. In *2021 Symposium on VLSI Circuits* (pp. 1-2). IEEE.

[19] Kim, D., Goldstein, B., Tang, W., Sigworth, F.J. and Culurciello, E., 2012. Noise analysis and performance comparison of low current measurement systems for biomedical applications. *IEEE transactions on biomedical circuits and systems*, *7*(1), pp.52-62.

[20] Kundert, K., 2006. Simulating switched-capacitor filters with SpectreRF. *The Designer's Guide Community*, pp.1-25.

[21] Rothe, R., Cho, M., Choo, K., Jeong, S., Oh, S., Lee, J., Sylvester, D. and Blaauw, D., 2022. A Delta Sigma-Modulated Sample and Average Common-Mode Feedback Technique for Capacitively Coupled Amplifiers in a 192-nW Acoustic Analog Front-End. *IEEE Journal of Solid-State Circuits*, *57*(4), pp.1138-1152.

[22] Schreier, R., Silva, J., Steensgaard, J. and Temes, G.C., 2005. Design-oriented estimation of thermal noise in switched-capacitor circuits. *IEEE Transactions on Circuits and Systems I: Regular Papers*, *52*(11), pp.2358-2368.

[23] Ying, D. and Hall, D.A., 2021. Current sensing front-ends: A review and design guidance. IEEE Sensors Journal, 21(20), pp.22329-22346.

[24] Crescentini, M., Bennati, M., Carminati, M. and Tartagni, M., 2013. Noise limits of CMOS

current interfaces for biosensors: A review. *IEEE transactions on biomedical circuits and systems*, *8*(2), pp.278-292.

[25] Ferrari, G., Gozzini, F., Molari, A. and Sampietro, M., 2009. Transimpedance amplifier for high-sensitivity current measurements on nanodevices. *IEEE Journal of Solid-State Circuits*, *44*(5), pp.1609-1616.

[26] Gan, R., Lyu, L., Mu, G. and Shi, C.J.R., 2022, April. A Neural Recording Analog Front-End with Exponentially Tunable Pseudo Resistors and On-Chip Digital Frequency Calibration Loop Achieving 3.4% Deviation of High-Pass Cutoff Frequency in 5-to-500 Hz Range. In *2022 IEEE Custom Integrated Circuits Conference (CICC)* (pp. 1-2). IEEE.

[27] Rothe, R., Oh, S., Choo, K., Jeong, S., Cho, M., Sylvester, D. and Blaauw, D., 2020, June. Sample and average common-mode feedback in a 101 nW acoustic amplifier. In *2020 IEEE Symposium on VLSI Circuits* (pp. 1-2). IEEE.

[28] Livanelioglu, C., Choi, W., Kim, D., Liao, J., Incandela, R., Cristiano, G. and Jang, T., 2022, June. A 0.0014 mm 2, 1.18 TΩ Segmented Duty-Cycled Resistor Replacing Pseudo-Resistor for Neural Recording Interface Circuits. In *2022 IEEE Symposium on VLSI Technology and Circuits (VLSI Technology and Circuits)* (pp. 62-63). IEEE.ben

[29] Switched Capacitor Circuits, Swarthmore College course notes. [Online]. Available: https://cheever.domains.swarthmore.edu/Ref/FilterBkgrnd/SwitchedCap.html

[30] Schreier, R., Silva, J., Steensgaard, J. and Temes, G.C., 2005. Design-oriented estimation of thermal noise in switched-capacitor circuits. *IEEE Transactions on Circuits and Systems I: Regular Papers*, *52*(11), pp.2358-2368.

[31] Boris Murmann, 2011, Noise Analysis in Switched-Capacitor Circuits. [Online]. Available: https://picture.iczhiku.com/resource/eetop/ShiFTilZDiTktncN.pdf

[32] Harpe, P., 2018. A compact 10-b SAR ADC with unit-length capacitors and a passive FIR filter. *IEEE Journal of Solid-State Circuits*, *54*(3), pp.636-645.

[33] Zhou, Z. and Warr, P., 2020. Feedback controlled pseudo resistor. *Electronics Letters*, *56*(8), pp.371-373.

[34] Sharma, K., Pathania, A., Pandey, R., Madan, J. and Sharma, R., 2021. MOS based pseudo-resistors exhibiting Tera Ωs of Incremental Resistance for biomedical applications: Analysis and proof of concept. *Integration*, *76*, pp.25-39.

[35] Seok, C., Lim, K., Seo, J., Kim, H., Im, S., Kim, J.H., Kim, C.Y. and Ko, H., 2013, October. Area-efficient RC low pass filter using T-networked resistors and capacitance

multiplier. In *2013 13th International Conference on Control, Automation and Systems (ICCAS 2013)* (pp. 1308-1311). IEEE.